

# AD-A278 567



## ATION PAGE

Form Approved  
GMP No. 0704-0136



1. AGENCY USE ONLY (Leave blank)		2. REPORT DATE March 24, 1994	3. REPORT TYPE AND DATES COVERED Reprint
4. TITLE AND SUBTITLE An Application of an Explicit Microphysics Mesoscale Model to a Regional Icing Event			5. FUNDING NUMBERS PE 61102F PR 2310 TA G7 WU 12
6. AUTHOR(S) George D. Modica, Scot T. Heckman, Roy M. Rasmussen*			
7. PERFORMING ORGANIZATION NAME(S) AND ADDRESS(ES) Phillips Lab/GPAP 29 Randolph Road Hanscom AFB, MA 01731-3010		8. PERFORMING ORGANIZATION REPORT NUMBER  PL-TR-94-2069	

9. PROWESSING AND/OR DISTRIBUTION STATEMENT	10. SECURITY CLASSIFICATION
---	-----------------------------

\*National Center for Atmospheric Research, Boulder, Colorado  
 Reprinted from Journal of Applied Meteorology, Vol. 33, No. 1, January 1994

Approved for public release; Distribution unlimited

**DTIC**  
**SELECTE**  
**S MAR 29 1994 B D**

A hydrostatic regional prediction model is modified to permit the existence of both liquid and ice hydrometeors within the same grid volume. The modified model includes an efficient ice-water saturation adjustment and a simple procedure to create or remove cloud water or ice. The objective was to determine whether such a model could provide deterministic forecasts of aircraft icing conditions in the 6-36-h period. The model was used to simulate an orographically forced icing event (the Valentine's Day storm of 12-14 February 1990) that occurred during the 1990 phase of the Winter Icing and Storms Project (WISP-90). Output from a 24-h nested-grid integration of the model was compared to observations taken during WISP-90. The model produced a thin (~1-2 km deep) supercooled liquid water (SLW) cloud that was in good agreement with observations in terms of initiation, duration, liquid water content, and location. Results of the simulation also suggest that slantwise ascent can be an important component in the production of SLW.

14. SUBJECT TERMS Aircraft icing, Microphysics, Numerical weather prediction, Winter icing and storms Project, Supercooled liquid water			15. NUMBER OF PAGES 10
			16. PRICE CODE
17. SECURITY CLASSIFICATION OF REPORT UNCLASSIFIED	18. SECURITY CLASSIFICATION OF THIS PAGE UNCLASSIFIED	19. SECURITY CLASSIFICATION OF ABSTRACT UNCLASSIFIED	20. LIMITATION OF ABSTRACT SAR

**Best  
Available  
Copy**

**An Application of an Explicit Microphysics Mesoscale Model to a Regional Icing Event**

GEORGE D. MODICA AND SCOT T. HECKMAN

*Atmospheric Sciences Division, Geophysics Directorate, Phillips Laboratory, Bedford, Massachusetts*

ROY M. RASMUSSEN

*National Center for Atmospheric Research, Boulder, Colorado\**

(Manuscript received 16 December 1992, in final form 25 July 1993)

## ABSTRACT

A hydrostatic regional prediction model is modified to permit the existence of both liquid and ice hydrometeors within the same grid volume. The modified model includes an efficient ice-water saturation adjustment and a simple procedure to create or remove cloud water or ice. The objective was to determine whether such a model could provide deterministic forecasts of aircraft icing conditions in the 6–36-h period. The model was used to simulate an orographically forced icing event (the Valentine's Day storm of 12–14 February 1990) that occurred during the 1990 phase of the Winter Icing and Storms Project (WISP-90). Output from a 24-h nested-grid integration of the model was compared to observations taken during WISP-90. The model produced a thin (~1–2 km deep) supercooled liquid water (SLW) cloud that was in good agreement with observations in terms of initiation, duration, liquid water content, and location. Results of the simulation also suggest that slantwise ascent can be an important component in the production of SLW.

BPJ



94-09571

**1. Introduction**

Aircraft icing research has relevance both to civilian and military aviation. Aircraft icing continues to be one of the primary causes of accidents among civilian aviation aircraft and is a concern for the military, which has requirements for high-performance aircraft operations in potential icing environments. The U.S. Air Force, for example, has turned to low-level flight as a means of increasing the survivability of its aircraft during certain tactical operations. Yet such operations can leave the aircraft vulnerable to icing since the amount of moisture generally increases with decreasing height. Therefore, both the military and civilian aviation communities stand to benefit from the accurate prediction of aircraft icing conditions.

The methods and techniques currently used by the air force to predict aircraft icing were developed mainly in the 1950s, with some later refinements (Air Weather Service 1980). These methods are subjective and time consuming. However, enormous advances in theory and computer power have made possible the use of sophisticated numerical weather prediction (NWP)

models to predict objectively the timing, location, and intensity of icing events.

In the last two decades alone, cloud microphysics research has progressed in earnest (see Lin et al. 1983). One result is that many of the identified complex microphysical processes are now successfully treated explicitly within cloud-scale prediction models. Unfortunately, these models often require enormous computational resources—even for horizontal domains of only hundreds of kilometers—since they typically utilize time-consuming parameterizations such as free atmosphere radiation, explicit nucleation, etc.

It is also true that considerable research on limited-area or regional numerical models has yielded impressive gains in the forecast skill of mesoscale motions (Anthes 1983). These gains have occurred despite the wide use within these models of highly parameterized moist physics. Only recently have efforts been directed toward merging these two areas of model formulation. This includes the application of explicit microphysical formulations within regional models having grid spacing of 10–50 km (e.g., Hsie et al. 1984; Zhang 1989). In this report, we describe a microphysics parameterization that utilizes some formulations developed for use within cloud-scale prediction models. The parameterization is next incorporated within a regional hydrostatic prediction model that is then used to simulate the events surrounding an icing event that occurred on 13–15 February during the 1990 Winter Icing and Storms Project (WISP-90). The WISP project deployed

\* The National Center for Atmospheric Research is sponsored by the National Science Foundation.

Corresponding author address: George D. Modica, PL/GPAP, 29 Randolph Rd., Hanscom AFB, MA 01731-3010.

94 3 28 116

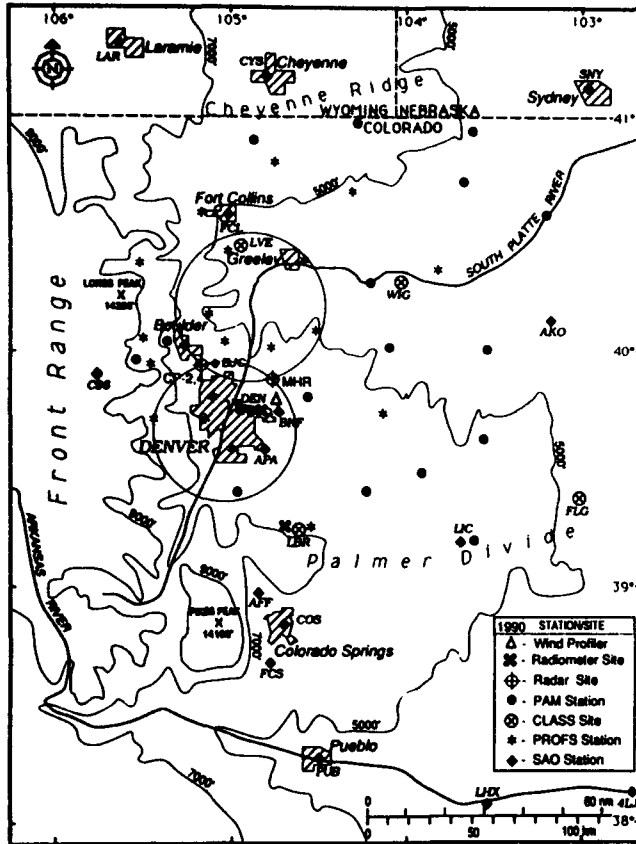


FIG. 1. Winter Icing and Storm Project 1990 (WISP-90) domain and network of instruments showing the location of various sensing systems. Topographic contours are given every 2000 ft (from Rasmussen et al. 1992).

a number of instruments to document the 1990 storm environment. These included Doppler radars (CP-3 and Mile High radars), aircraft (University of Wyoming King Air and the University of North Dakota Citation), radiometers, mesonet stations [Portable Automated Mesonet (PAM) and Program for Regional Observing and Forecast Services (PROFS)], and Cross-chain Loran Atmospheric Sounding System (CLASS) observations (Fig. 1). Additional data were obtained from wind profilers, National Weather Service soundings, and satellites. The main goals of WISP are to 1) study and improve our understanding of the dynamical and microphysical processes leading to the formation and depletion of supercooled liquid water (SLW) in winter storms, and 2) improve forecasts of aircraft icing. It is hoped that parameterizations like the one described here will eventually contribute toward the attainment of these goals.

In the next section, the NWP model is described. Special attention is given to the treatment of the model's microphysics. Section 3 provides some of the details of the initial data used in the study. Section 4 focuses on the synoptic setting of the 13–15 February icing

event. Finally, we present some results and discussion in section 5, and conclusions in section 6.

## 2. Numerical model

The model used in this study was a modified version of one developed originally by the National Center for Atmospheric Research and The Pennsylvania State University (Anthes and Warner 1978; hereafter referred to as the NCAR-PSU model). The modified version was essentially the same as that detailed in Zhang (1989)—hereafter referred to as Z89—and is summarized in Table 1. The relevant differences between Z89 and our version are described next.

The explicit moisture scheme in Z89 accounts for the effects of virtual temperature, hydrostatic water loading, and the condensation, evaporation, freezing, melting, and sublimation of hydrometeors. Furthermore, autoconversion and accretion processes are represented but riming is not. However, unlike Z89 where the phase demarcation between liquid water (i.e., cloud water and rainwater) and frozen particles (i.e., cloud ice and snow crystals) was made to be dependent upon the position of the parcel above or below the 0°C isotherm, the modified version permitted liquid and frozen particles to coexist between 0°C and some arbitrary lower temperature (−40°C in this study). In order to facilitate a reversal of the above limitation, an efficient ice–water saturation adjustment (Tao et al. 1989) was added that permitted calculation of adjusted temper-

TABLE 1. Features of the NCAR-PSU model, version 4

Domain	
horizontal	Two-way interactive nested grid (Zhang et al. 1986); coarse grid mesh (CGM) $83 \times 83$ , $\Delta x = 30$ km; fine grid mesh (FGM) $79 \times 79$ , $\Delta x = 10$ km. CGM and FGM centered at $39.75^\circ\text{N}$ , $104.86^\circ\text{W}$ (Denver, Colorado); staggered (Arakawa B) grid.
vertical	Staggered; variable resolution, terrain-following coordinate ( $\sigma$ ); 29 levels with approximately 10 levels in lowest 1 km and 50-mb spacing thereafter; $p_{\text{top}} = 50$ mb.
Numerics	Hydrostatic; leapfrog, $\Delta t = 45$ (15) s for CGM (FGM); pressure averaging, time smoothing; fourth-order advection and deformation-dependent horizontal diffusion; relaxation lateral boundary condition (Davies and Turner 1977) for the CGM.
Turbulence modeling	First-order closure ( $K$ theory) for stable module, nonlocal plume scheme for unstable module; high-resolution PBL (Zhang and Anthes 1982).
Convection	Modified Kuo (Anthes 1977) on CGM only.
Microphysics	Bulk; five categories of predicted water: vapor, liquid cloud, ice cloud, liquid precipitation, frozen precipitation (Zhang 1989); ice–water saturation adjustment (Tao et al. 1989); liquid–frozen cloud partitioning (Lord et al. 1984).

ature and mixing ratio in the presence of any combination of ice cloud and liquid cloud. The phase of cloud ultimately produced (or depleted) is determined with the aid of the following two assumptions used by Lord et al. (1984). 1) The saturation mixing ratio  $q_{vs}$  is defined as a mass-weighted average of the saturation values over liquid water  $q_{ws}$  and ice  $q_{is}$  between  $0^\circ\text{C}$  and the predefined lower temperature,

$$q_{vs} = \frac{q_c q_{ws} + q_i q_{is}}{q_c + q_i}, \quad (1)$$

where  $q_c$  and  $q_i$  are cloud liquid and ice mixing ratios, respectively. 2) If the grid volume is determined to be supersaturated (see Tao et al. 1989 for details), then the excess water vapor is converted to cloud water and/or ice. Between  $0^\circ\text{C}$  and the predefined lower temperature the partitioning between newly formed cloud water/ice is linearly dependent on the temperature, such that

$$\Delta q_c = -\Delta q_v \left( \frac{T - T_{00}}{T_0 - T_{00}} \right) \quad (2)$$

and

$$\Delta q_i = -\Delta q_v \left( \frac{T_0 - T}{T_0 - T_{00}} \right), \quad (3)$$

where  $T_0 = 0^\circ\text{C}$  and  $T_{00}$  is set to  $-40^\circ\text{C}$  for this experiment. If the grid volume is subsaturated, excess cloud water (if any) is evaporated before cloud ice due to the higher vapor pressure of liquid water relative to that of ice. The second assumption implies there is always a sufficient number of condensation-ice-activation nuclei present to remove any supersaturation.

While the definition of  $T_{00} = -40^\circ\text{C}$  might at first seem arbitrary, it is not quite as arbitrary as it appears, for the following reasons. First, recent aircraft- and ground-based lidar studies have revealed the presence of SLW at temperatures approaching  $-40^\circ\text{C}$  at the base of cirrostratus clouds (Sassen et al. 1985; Sassen et al. 1990). We did not want to preclude the formation of SLW at these temperatures in our simulation knowing that this observational evidence exists. Second, choosing  $T_{00} > -40^\circ\text{C}$  would have inadvertently partitioned the cloud into a greater fraction of ice in contrast with observations taken during this case. This is precisely why Tao et al. (1989) suggested the use of aircraft data to help determine the best value of  $T_{00}$ . The important point to recognize here is that the simplicity of the saturation adjustment used in this model necessitates some ad hoc compromises in the treatment of the microphysics. The cloud partitioning implied by Eqs. (2) and (3) with  $T_{00} = -40^\circ\text{C}$  may not be appropriate for all cases but seems to be a good choice for the conditions observed in this case.

Another distinguishing feature of the present model is that it permits more than one melting-freezing layer

in a vertical column whereas the version in Z89 permitted only one. This capability becomes essential as increasingly higher vertical resolution raises the possibility of resolving more than one freezing level. All liquid cloud and rain that is transported above the  $T_{00}$  level will freeze. (Note that rain at  $T_{00} = -40^\circ\text{C}$  is improbable and was essentially nonexistent at these temperatures in the simulation.) All frozen cloud and snow that is transported below the  $0^\circ\text{C}$  level will melt. These processes may occur wherever such interfaces exist in the model in the presence of vertically moving hydrometeors. Melting and/or freezing is assumed to occur within a single model layer. This could pose a problem if too much frozen precipitation were to fall through a melting layer that was close to the ground where the model's vertical resolution is very high. An inadvertent result of the formulation in this model (and that in Z89) could be to concentrate the diabatic cooling over an unrealistically shallow layer, whereas in the real atmosphere the precipitation would likely melt throughout a depth equivalent to two or more model layers. However, this particular case was characterized by low precipitation rates so that the above scenario did not create serious problems in this simulation.

Almost any simulation on the coarse grid mesh (CGM,  $\Delta x = 30$  km) will need some way to represent subgrid-scale convective processes; this requires a convective parameterization. We chose to activate on the CGM both the convective parameterization (Anthes 1977) and the explicit microphysics. This configuration was determined by Zhang et al. (1988) to allow a broader-scale interaction between the parameterized convection and mesoscale environment and to have the greatest potential success in predicting mesoscale precipitating weather systems that occur under various environmental conditions. However, for the fine grid mesh (FGM,  $\Delta x = 10$  km) we must recognize that some of the assumptions of the convective parameterization begin to break down as the grid size approaches the horizontal scale of the convection-driven circulations (Pleim et al. 1991). Therefore, on the FGM we have chosen to activate the explicit microphysics only. This is a departure from the model in Z89, which makes use of the Fritsch and Chappell (1980) cumulus parameterization on the FGM.

A final question one should first ask before deciding to proceed with the use of cloud microphysics parameterizations such as the one described above is, "What is their applicability to mesoscale models?" After all, as Hsie and Anthes (1984) noted, these parameterizations were developed for very high resolution cloud models and as such may not be appropriate for mesoscale models.

On the other hand, when the grid spacing in mesoscale numerical models is reduced below 50 km, some of the assumptions are no longer valid in these same models' cumulus parameterization schemes. For example, the  $b$  factor in Kuo's (1974) scheme, which

determines the relative amounts of precipitation and storage, may depend on grid size or the nature of the precipitation (Hsie and Anthes 1984).

We are then left with a decision to make regarding the selection of methods to parameterize the salient moist physical processes observed during this case. To assist in this decision-making process, we note the following: first, we hypothesize that the microphysics parameterizations under consideration here, while maybe not perfectly suited to mesoscale models, will represent grid-resolvable moist physical processes better than the alternative, which is to neglect microphysics completely. Second, the explicit microphysics scheme used in the NCAR-PSU model and detailed in Z89 has been used with success for a variety of meteorological systems, from midlatitude fronts and squall lines to extratropical cyclones (e.g., Hsie et al. 1984; Zhang et al. 1988; Kuo and Low-Nam 1990). We have interpreted these successes as a confirmation of the explicit microphysics scheme's validity on scales much larger than cloud scale.

### 3. Initial data

In preparation for a 24-h simulation beginning 1200 UTC 13 February 1990, we prepared an initial analysis as follows. Between 55 and 70 NWS rawinsondes and over 600 NWS surface observations valid 0000 UTC 13 February were objectively analyzed on an expanded grid to provide gridded values to the CGM shown in Fig. 2. (The expanded grid is illustrated in Fig. 3.) The objective analysis procedure uses a Cressman-type scheme (Benjamin and Seaman 1985) in which several

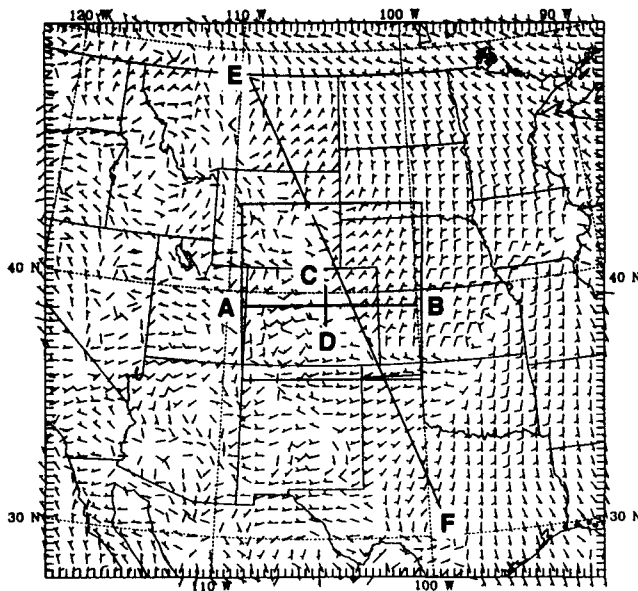


FIG. 2. Analyzed surface wind field on CGM valid 1200 UTC 13 February 1990. Half and full barbs represent 5 and 10  $\text{m s}^{-1}$ , respectively. Labeled lines denote orientation of cross sections. Position of FGM shown by inner square.

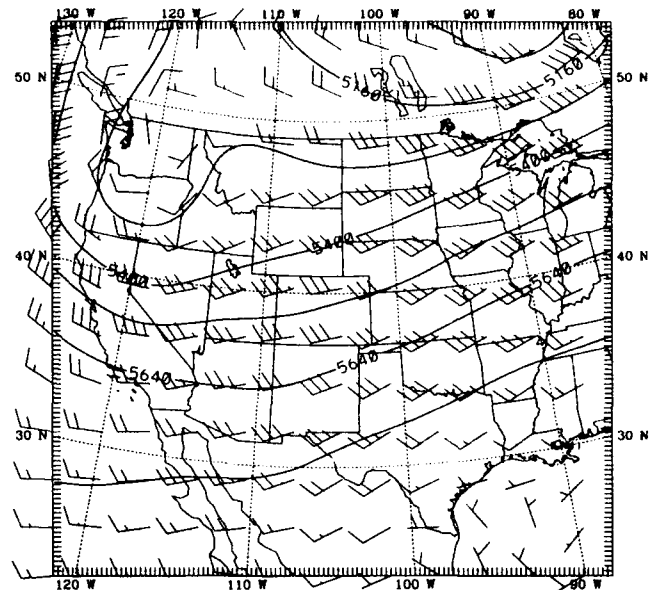


FIG. 3. NMC analyzed 500-mb height field (m) on the expanded grid, valid 1200 UTC 13 February 1990, with contours every 120 m and wind vectors with half and full barbs equal to 5 and 10  $\text{m s}^{-1}$ , respectively.

scans nudge a gridded first-guess field on pressure surfaces toward the observations. A  $2.5^\circ \times 2.5^\circ$  gridded analysis generated by the National Meteorological Center (NMC) was used as a first guess for this analysis. A 10' terrain dataset provided surface elevation. An implicit nonlinear normal-mode initialization (Errico and Bates 1988) was then used to reduce large-amplitude gravity-inertia wave activity during the early stages of the forecast. The initialization procedure essentially modifies the analyzed data so as to satisfy a dynamic balance condition. Next, the model was run to produce a 12-h forecast on the CGM valid 1200 UTC 13 February. Finally, a second objective analysis was performed with 1200 UTC data. This analysis differed from the first in three ways. 1) The 12-h CGM forecast valid 1200 UTC 13 February was used as the first guess for the analysis. 2) The upper-air portion of the analysis included four CLASS soundings taken during this WISP observing period. 3) The initialization step was omitted. The model was then run with both the CGM and the FGM for an additional 24 h to 1200 UTC 14 February 1990.

### 4. Synoptic discussion

Between 0000 UTC 13 February and 0000 UTC 14 February 1990, a shallow dome of cold air associated with a Canadian high pressure system moved southward, east of the Colorado Front Range. At about 0900 UTC 13 February, a shallow upslope cloud of supercooled liquid water (SLW) had formed east of the Front Range within low-level easterly flow. Throughout this period, there was southwesterly to southerly flow aloft.

This condition persisted for three days and has become known as the Valentine's Day storm (Rasmussen et al. 1991). During the first two days, this storm was observed to produce and maintain a widespread area of supercooled liquid water. Snowbands developed on the third day (Rasmussen et al. 1992). Daily maximum surface temperatures—valid for a 24-h period ending 0000 UTC—dropped over 40°F at some Front Range stations (66° to 26°F at DEN) during the two consecutive days of 13 and 14 February. Overall precipitation rates and amounts were generally small during this time. Some specific details of this case are discussed next.

A digging 500-mb trough, with its axis aligned with the Pacific coast at 1200 UTC 12 February 1990, continued to deepen and gradually form a cutoff over the Oregon–Washington border by 1200 UTC 13 February (Fig. 3). After this time the cutoff pushed southeastward, passing just to the west of Salt Lake City by 1200 UTC 14 February and continued on to the Four Corners area by 1200 UTC 15 February. Consequently, the upper-air flow above the Front Range throughout this period was generally southwesterly. At the surface during this time, the flow associated with the Canadian high pressure system was northeasterly and gradually became more easterly as it approached the Rocky Mountains (Fig. 2). Immediately to the east of the Front Range and just above the surface, there was a northerly low-level jet as is often observed in many cold-air damming cases. This jet is shown in Fig. 4, which is a cross section along line AB on the FGM shown in Fig. 2. Since the terrain east of the Front Range slopes up gradually from east to west there was orographic lifting and, hence, isentropic cooling of the easterly flow near the surface. This cooling was suffi-

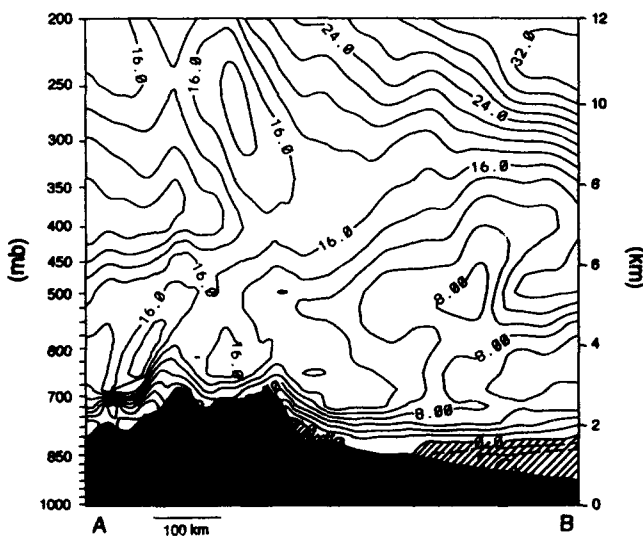


FIG. 4. East–west cross section on the FGM of 6-h forecast  $v$  component of velocity ( $\text{m s}^{-1}$ ) along line AB in Fig. 3 valid 1800 UTC 13 February 1990. Contour interval is  $2 \text{ m s}^{-1}$ . Negative values (northerly winds) are displayed as hatched areas.

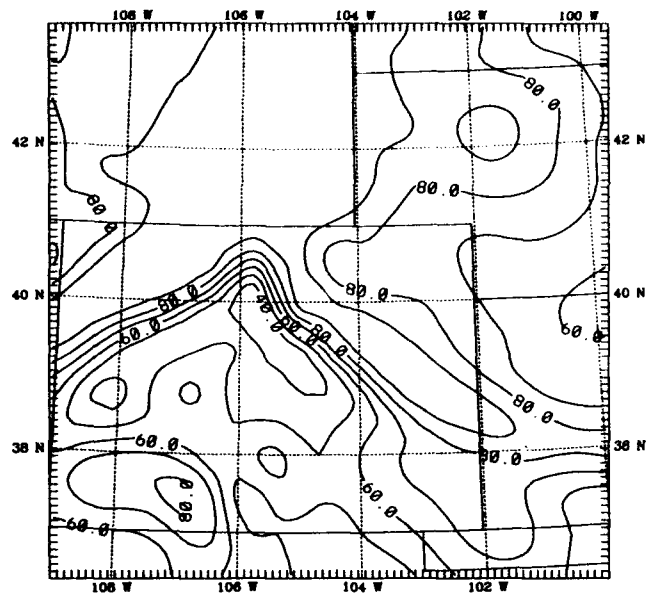


FIG. 5. FGM analyzed field of surface relative humidity (%), contours every 10%. Valid 1200 UTC 13 February 1990.

cient to saturate the fairly low amounts of vapor ( $\sim 2 \text{ g kg}^{-1}$ ) in this polar continental air mass (Fig. 5). As mentioned earlier, an upslope cloud developed in the vicinity of the WISP-90 observational network at 0900 UTC 13 February—7 h after the passage of the initial cold front from the northeast. This cloud persisted for well over 48 h. Figure 6 is a visible satellite image from 1800 UTC 13 February centered over the WISP-90 domain. The broad area of this orographic cloud is evident along the north–south extent of the Front Range as well as over northeastern Colorado. The orographic cloud appears as a very smooth feature with almost no discernible embedded detail. Not surprisingly, the orographic lifting was confined to a thin layer just above the surface so that the clouds east of the Front Range were very shallow. This shallow cloud will be discussed further in the next section. Analysis of mesonet data (PAM and PROFS) revealed a secondary surge of arctic air through the region at about 1400 UTC 13 February (Rasmussen et al. 1992). When the secondary cold front encountered the north slope of the Palmer Divide, it stalled and remained there until about 0000 UTC 14 February. This stalled front presented an opportunity for the research aircraft to sample a nearly steady-state SLW cloud structure. Rasmussen et al. (1992) estimated the vertical velocities associated with frontal lifting of the southerly wind above this surface front and found them to be greater than those due to the orography below by an order of magnitude. Frontal lifting along the broader upper-air front appeared to be related to an elevated layer of cloud oriented southwest–northeast that intersected the Front Range near the Colorado–Wyoming border and then extended across the South Dakota–Nebraska bor-

der and into southern Minnesota. This layer is apparent in the satellite image as a cloudy region with embedded convective features extending southwest–northeast across the northern half of the picture. Infrared satellite imagery (not shown) revealed brightness temperatures at these cloud tops that would place their height close to 500 mb. Finally, a third cold-air surge passed through the network just after 0000 UTC 14 February, pushing the SLW cloud south and replacing it with a frozen precipitation regime.

## 5. Results and discussion

The model was able to simulate the meaningful large-scale features on the CGM with acceptable accuracy. The evolution of the simulated upper-air trough and the progression of the surface high pressure system were in good agreement with observations during the 36-h simulation. The model was also able to reproduce many important small-scale features. Precipitation forecasts can be a good proxy for the overall performance of the model since the precipitation pattern and amounts are attributable to many different scales and effects. Figure 7 shows both the observed 24-h cumulative precipi-

tation amounts and those for the FGM simulation valid 1200 UTC 14 February. The overall simulated precipitation coverage is similar to the observed, with the possible exception of the southwest quadrant of Colorado where the model precipitation appears overdone. (Note, however, that there were few precipitation reports west of the Continental Divide with which to verify the simulated precipitation.) Nonetheless, there are two main axes of precipitation maxima evident in both the observed and simulated patterns. The first is a northwest–southeast precipitation maxima on the CGM (not shown) that is aligned with the Front Range of Montana, Wyoming, and Colorado. This maximum was caused by the orographic lifting of the low-level easterly flow associated with the Canadian high pressure system as it encountered the abrupt terrain height increase of the Front Range. A second (and less distinct) precipitation maxima is oriented nearly perpendicular to the first and extends southwest–northeast over the Colorado–Wyoming border. This precipitation maximum appears to be associated with frontal lifting of southwesterly air over the cold northeasterly surface flow as this axis is oriented parallel to the general 500-mb flow at this time. The precipitation rates (water

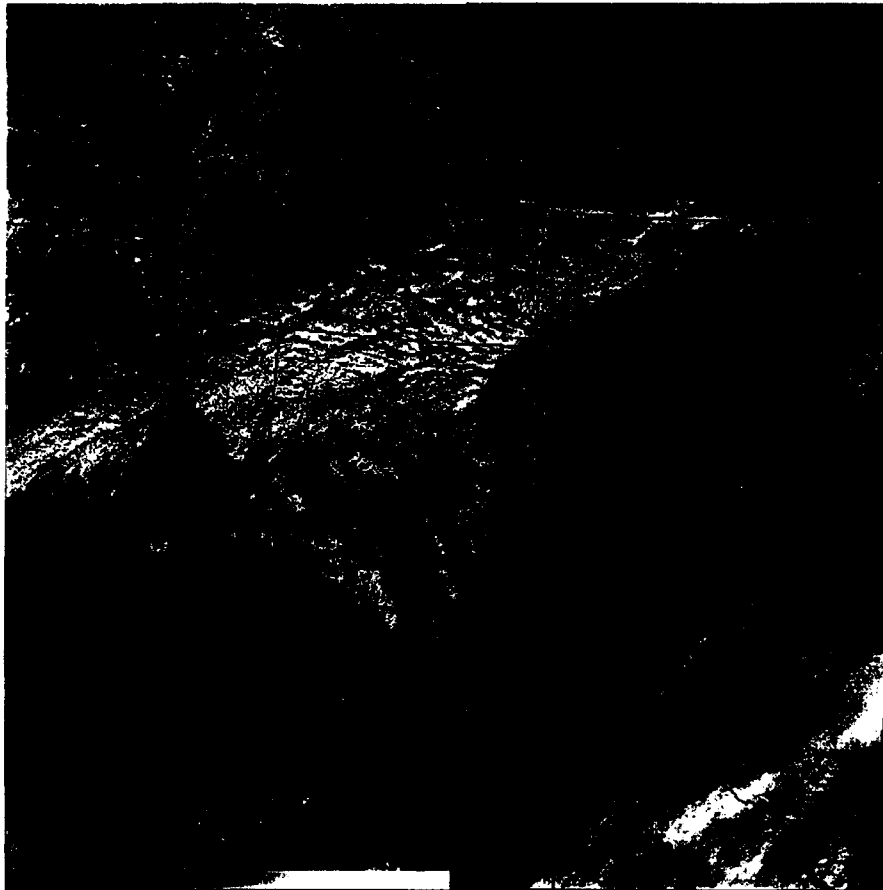


FIG. 6. Visible satellite image with coverage of the WISP-90 domain valid 1800 UTC 13 February 1990.

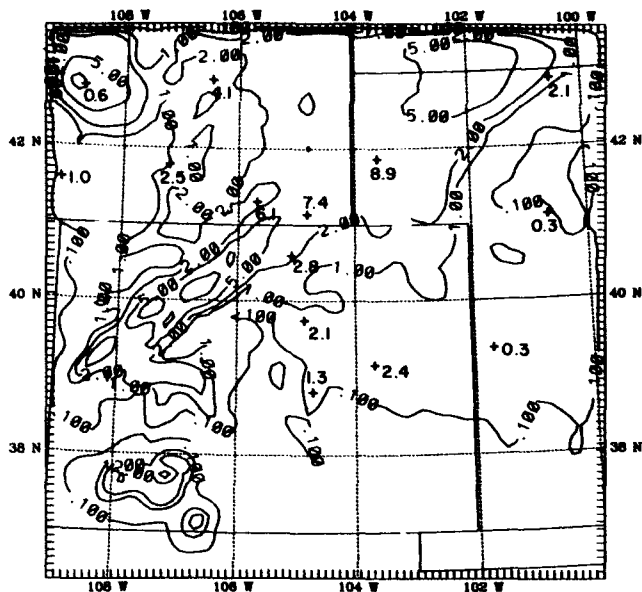


FIG. 7. Twenty-four-hour accumulated precipitation (mm) valid 1200 UTC 14 February 1990 from from a 24-h simulation on the FGM and that observed from the available surface reporting stations (denoted with a plus).

equivalent) in the vicinity of the orographic cloud were very low or even nonexistent because of the thermodynamic stability of this dome of cold air.

The surface wind field was strongly affected by the various terrain features in the WISP-90 domain. Figure 8 shows the simulated surface wind field for a 12-h FGM forecast valid 0000 UTC 14 February. The clockwise flow around the surface high is evident in the eastern half of the FGM domain. This easterly flow pattern, along with the underlying terrain slope of the Great Plains, is responsible for the orographic lifting and consequent formation of the low-level SLW cloud. Note that near 40°N the easterly winds are deflected southward as they approach the Front Range. This is yet another perspective of the low-level jet discussed in the last section and shown in Fig. 4. Furthermore, Fig. 4 reveals how rapidly with height the winds reverse direction so that minor variations in terrain height translate into significantly different wind environments. This is evident in Fig. 8 as well: note that the Palmer Divide and the Cheyenne Ridge (see Fig. 1 for reference) are regions of higher elevation. The South Platte River valley lies between these two features and marks a minimum in the (north-south) terrain field. As one proceeds from south to north just west of 104°W in Fig. 8, note that the winds become more southerly over both the Palmer Divide and the Cheyenne Ridge. The combination of the northerly low-level jet located west of Denver and discussed above, the easterly flow over the South Platte River valley, the southerly flow over the Palmer Divide, and the westerly flow over the mountainous elevations to the west combine to produce a closed circulation whose center is visible to the

south of Mile High Radar (MHR) in Fig. 8. This feature has been named the Denver Cyclone (Szoke et al. 1984) and is often observed near the Denver area when the airflow in the vicinity of the Palmer Divide has a southerly component. At 2000 UTC 13 February, the WISP-90 surface mesonet observed the closed circulation pattern shown in Fig. 9. (The area illustrated by this figure is outlined in Fig. 8 for reference.) The mesonet reveals the same southeasterly-easterly-southeasterly wind pattern as one proceeds from south to north as in the model simulation; this pattern corresponds to the higher elevation of the Palmer Divide, the elevation minimum of the South Platte River valley, and the higher elevation of the Cheyenne Ridge, respectively. The location of the observed Denver Cyclone corresponds closely to the position in the model simulation. The similarity between the observed and simulated surface wind fields raises the level of confidence in the model's ability to accurately provide input to the moist physics. It was not certain from the model simulation whether or not this circulation pattern had any effect on the evolving precipitation pattern. However, radar reflectivity data at this time (not shown) indicated a narrow curved band of enhanced reflectivity about 25 km in length and 5 km in width, located to the northeast of the circulation center.

Figure 10 shows a north-south vertical mean sea level (MSL) cross section (along line CD in Fig. 2) of cloud liquid water content derived from aircraft data collected between 1723 and 1928 UTC 13 February and that from the corresponding model simulation valid 0000 UTC 14 February. The observed cloud base

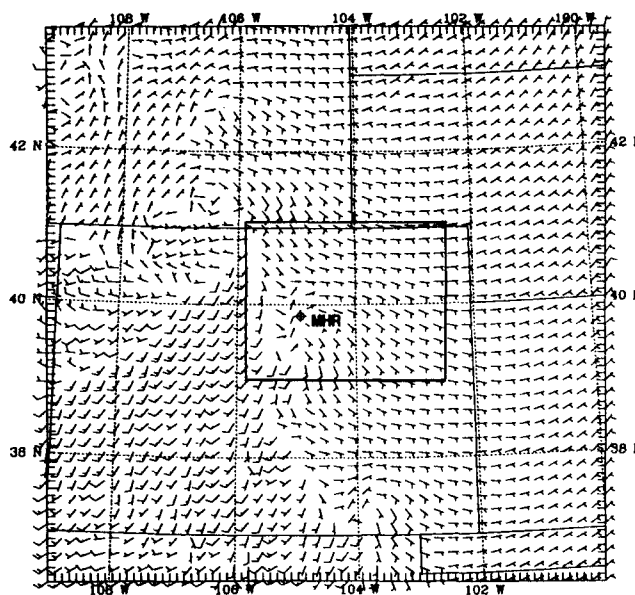


FIG. 8. Model-simulated surface winds ( $m s^{-1}$ ) from a 12-h forecast on the FGM valid 0000 UTC 14 February 1990 showing the Denver Cyclone south of Mile High Radar (MHR). Half and full barbs represent 5 and 10  $m s^{-1}$ , respectively. Area shown in Fig. 9 delimited by inner box.

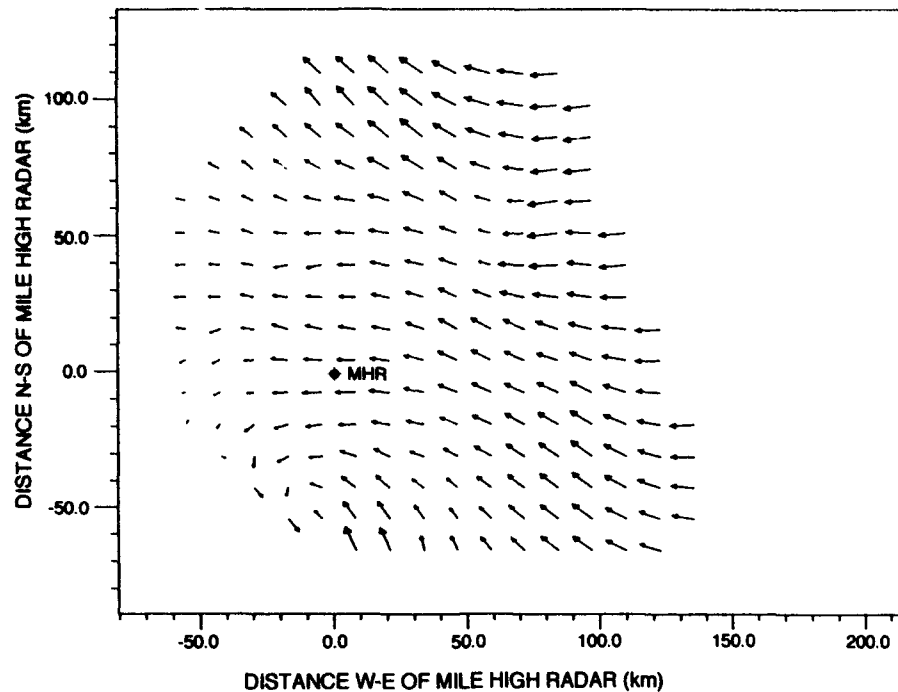


FIG. 9. WISP-90 surface mesonet winds ( $\text{m s}^{-1}$ ) from MHR valid 20 UTC February 1990 for region delimited in Fig. 8. Distances are kilometers from MHR. The closed circulation pattern of the Denver Cyclone is about 50 km south of MHR. Small-, medium-, and large-length vectors correspond to 5, 10, and  $15 \text{ m s}^{-1}$ , respectively.

was generally within a few hundred meters above ground level and the cloud depth was about 1 km. Note that the aircraft measurements for this case provide only a small geographic sample with which to verify against the model simulation. Nevertheless, the model forecast cloud of SLW compares well with the aircraft-observed cloud in terms of the heights of the cloud base and top. The simulated concentrations of liquid cloud water ( $\text{g kg}^{-1}$ ) are close to the observed values ( $\text{g m}^{-3}$ ). (For the range of temperatures and pressures in this region, grams per cubic meter are approximately equal to grams per kilogram within 10%.) The peak values of  $q_c$  in the simulation are not as high as those sampled by the aircraft. This may be partially explained by the fact that the simulated concentrations are averaged over a  $(10 \text{ km})^2$  grid. On the other hand, the aircraft was able to detect very small-scale features like the thin ( $\sim 400 \text{ m}$  deep) liquid water concentration maximum in the southernmost portion of Fig. 10a that probably was produced by the upglide of moist air to the south over the stationary frontal surface. The vertical grid spacing of the model (about 500 m at this height) was not sufficient to resolve this thin patch and instead may have smoothed it out; the simulation might also have shifted this feature out of the plane of the cross section.

The simulated thermal structure is in good agreement with observations in this region (Fig. 11). There was a shallow layer of subfreezing air with a strong

inversion at around 3200 m MSL. The model placed the simulated inversion slightly lower (2800 m MSL). Furthermore, the model placed its isotherm pattern about 35 km north of the observed pattern. The general observed wind pattern was reproduced in the simulation; in both cases there were light ( $\sim 5 \text{ m s}^{-1}$ ) east-southeast winds within the cold pool and south-southwesterly flow ahead of and near the level of the inversion. The wind speeds approached  $10\text{--}20 \text{ m s}^{-1}$  near the level of the inversion in both the simulation and in aircraft measurements.

Orographic forcing was not the only mechanism acting to produce clouds in the WISP-90 domain during the simulation. A second mechanism appeared to be important in the production of SLW. Figure 12 is a cross section of the 6-h forecast liquid cloud water along line *EF* (refer to Fig. 2), which lies normal to the 500-mb flow of this time. Note the northerly tilted orientation of the cloud and its vertical extent. This feature was part of a larger simulated structure that was oriented southwest-northeast as it intersected the Front Range in the north-central portion of the FGM and extended into northeastern Nebraska and southern Minnesota on the CGM (not shown). The observational evidence in Fig. 6 verifies the existence of this simulated cloud. Throughout its horizontal extent, the simulated cloud generally sloped upward from south to north as indicated in Fig. 12 and in infrared imagery (not shown). A majority of the cloud resided in the

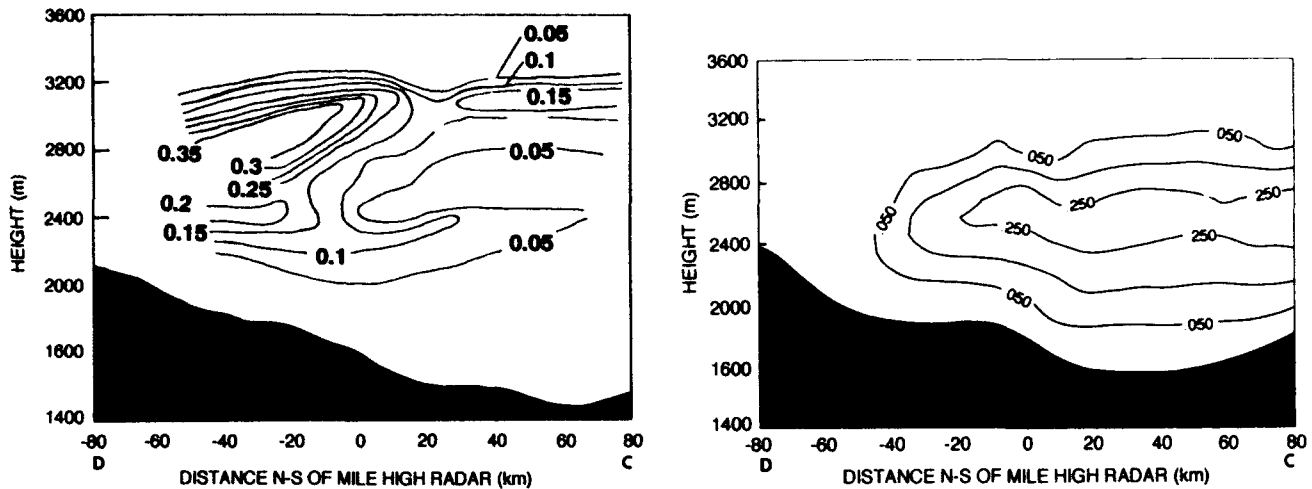


FIG. 10. North-south cross section of cloud liquid water content along line CD in Fig. 2; (a) observed values ( $\text{g m}^{-3}$ ) obtained from probes aboard the University of Wyoming King Air between 1723 and 1928 UTC 13 February 1990. Contour interval is  $0.05 \text{ g m}^{-3}$  starting at  $0.05 \text{ g kg}^{-1}$ ; (b) 12-h forecast cloud liquid water ( $\text{g kg}^{-1}$ ) from the FGM valid 0000 UTC 14 February 1990. Contour interval is  $0.1 \text{ g kg}^{-1}$  starting at  $0.05 \text{ g kg}^{-1}$ . [Note that for the ambient temperatures and pressures here, grams per cubic meter approximately equal grams per kilogram within 10%.]

layer between 600 and 500 mb with peak  $q_c$  concentrations ( $\sim 0.45 \text{ g kg}^{-1}$ ) closer to 625 mb. This particular cloud was still present in both the model simulation and in satellite imagery at 1200 UTC 14 February. Unfortunately, it is not possible to determine from either the satellite picture or aircraft measurements (which did not extend into this region) whether or not this cloud was in reality liquid or frozen, although from Fig. 6 it has more the appearance of a liquid altostratus cloud instead of a fuzzier ice cloud. Otherwise is difficult to determine with any greater certainty than that.

Since this feature is far from the surface and extends well to the east of the Rocky Mountains, it cannot be explained by orographic lifting, as was the case with

the low-level cloud below. Furthermore, a sounding from the Wiggins CLASS station at 1200 UTC 13 February (Fig. 13) shows that the troposphere at the time was stable to upright parcel displacements. Figure 14 shows the 6-h forecast (valid 1800 UTC 13 February) orientation of lines of constant  $\theta_e$  and absolute momentum  $M$  along the CGM cross section EF. A necessary prerequisite for slantwise convection is a decrease in  $\theta_e$  with height along a surface of constant  $M$  (Emanuel 1983). The region in Fig. 14 where this potential instability is evident is indicated by the shading. Note that within the shaded region there is a smaller enclosed area that is conditionally neutral to moist slantwise ascent. Comparison of the location of this smaller area with that of the cloud in Fig. 12 reveals that the cloud

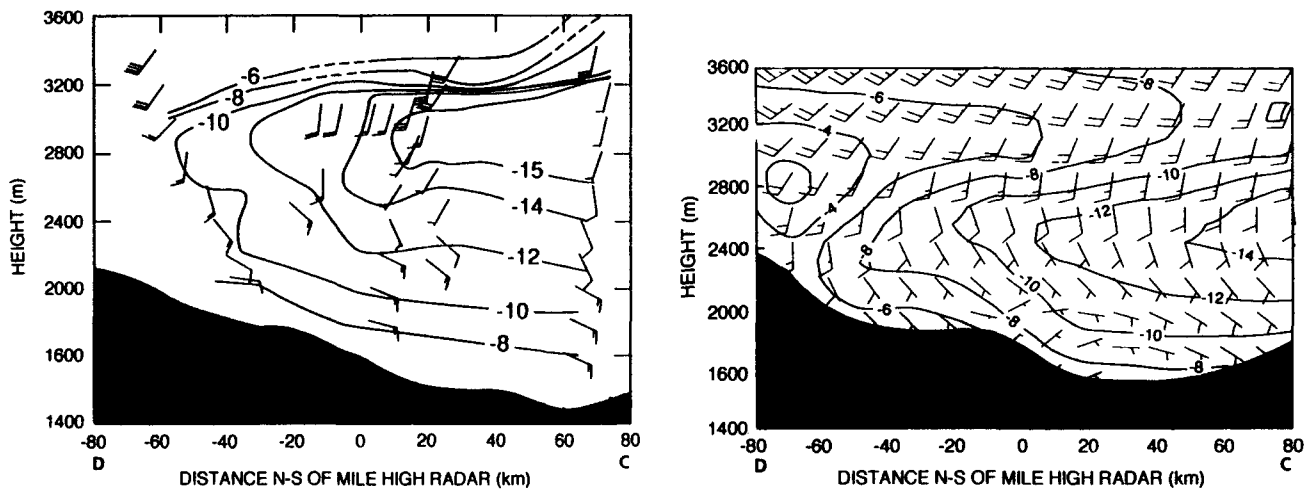


FIG. 11. Same as Fig. 10 except for temperature ( $^{\circ}\text{C}$ , contour interval is  $2^{\circ}\text{C}$ ), and horizontal wind represented as shaft and barbs. (a) Observed values; full barbs represent  $5 \text{ m s}^{-1}$ . (b) Forecast values; full barbs represent  $10 \text{ m s}^{-1}$ .

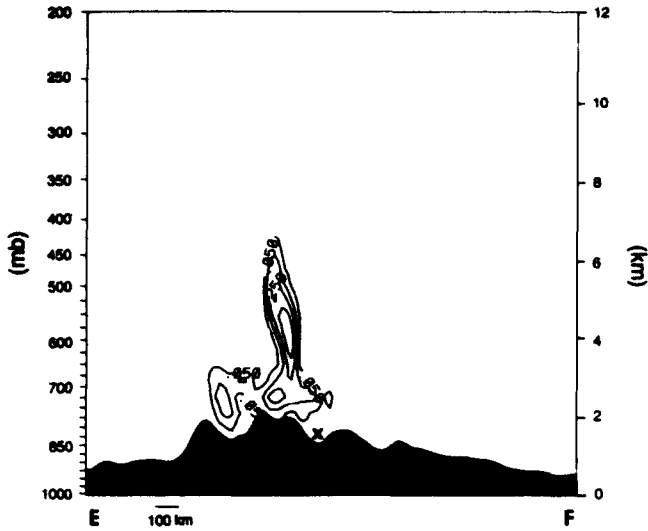


FIG. 12. Cross section of model-simulated cloud liquid water content ( $\text{g kg}^{-1}$ ) on the CGM along line EF for the 6-h forecast valid 1800 UTC 13 February 1990. Contour interval is  $0.1 \text{ g kg}^{-1}$  starting at  $0.05 \text{ g kg}^{-1}$ . The South Platte River valley is denoted by the cross.

generated by large-scale frontal ascent. The observed coexistence of slantwise conditional neutrality and potential instability was noted and discussed in Emanuel (1988) as evidence that slantwise moist convection acts to rapidly neutralize the instability generated by the large-scale motions. This simulation confirms that this process can be represented explicitly in a meso- $\beta$ -scale simulation with parameterized microphysics.

The mere existence of potential instability is not a sufficient condition for the instability to be realized. Another prerequisite is the presence of some kind of triggering mechanism to perturb the unstable parcels. West-east cross sections across the Front Range of vertical velocity and cloud water content (not shown) indicate that gravity wave-induced vertical motions above the Continental Divide, as the westerlies were lifted over the Rocky Mountains, may have been responsible for triggering the westernmost slantwise motions. These gravity-wave motions could continue to influence the structure of the SLW cloud several hundred kilometers downwind of the mountains, although it is unlikely they played an essential role in the overall development and maintenance of this feature at distances much beyond the Front Range.

occupies an area of slantwise conditional neutrality. Thus, it is quite possible that the parcel motions within this cloudy region are acting to neutralize the instability

The above result suggests that slantwise ascent can be an important component in the production of SLW

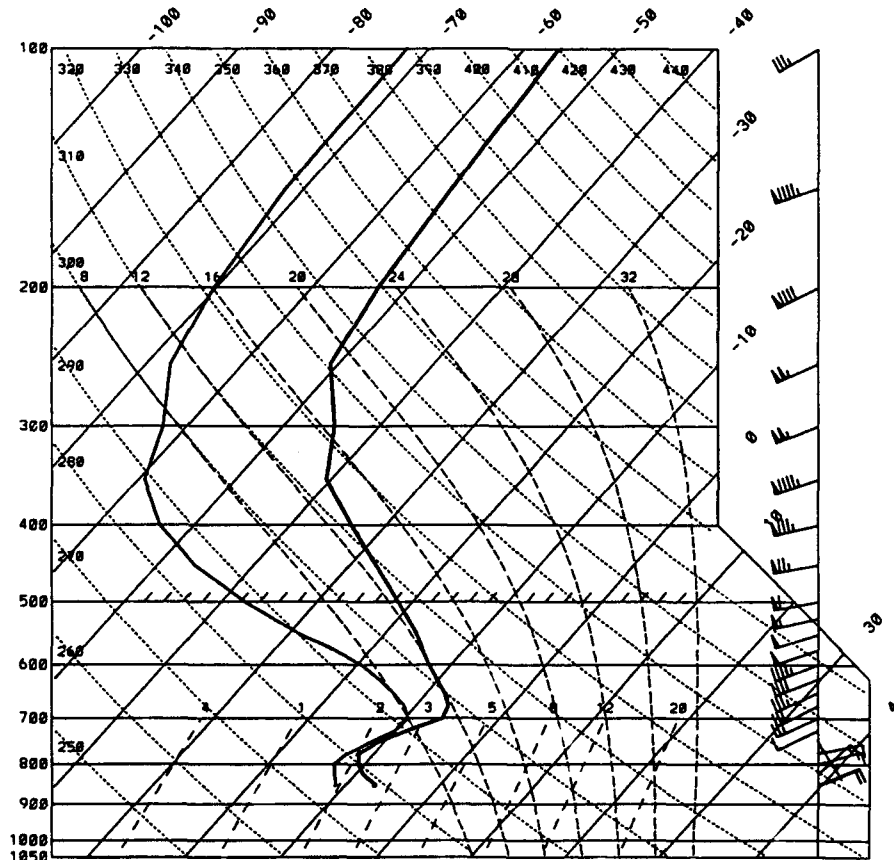


FIG. 13. CLASS sounding taken at Wiggins, Colorado, at 1200 UTC 13 February 1990.

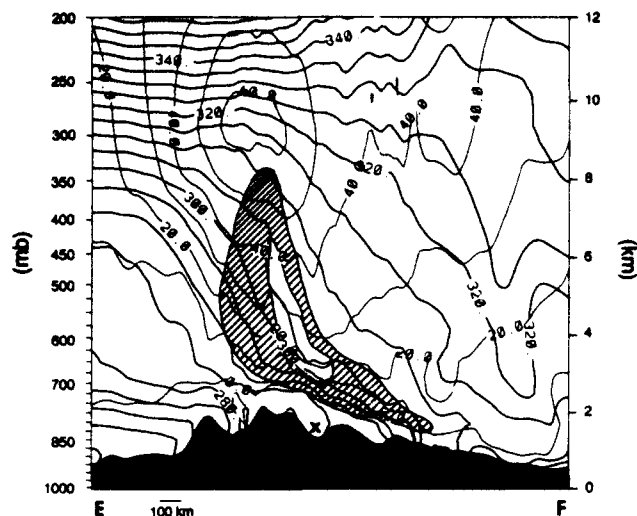


FIG. 14. Cross section of model-simulated  $\theta_e$  (K, thick contours every 5 K) and pseudo-angular momentum ( $\text{m s}^{-1}$ , thin contours every  $10 \text{ m s}^{-1}$ ) for a 6-h forecast along line EF valid 1800 UTC 13 February 1990. The area of slantwise potential instability is illustrated by hatching. The South Platte River valley is denoted by the the cross.

at higher levels in the troposphere; and therefore, a complete assessment of icing potential should include a check for this condition.

## 6. Conclusions

We have modified a regional-scale hydrostatic prediction model with the intent of providing it with the capability to simulate, among other things, the production and depletion of SLW. This entailed changes to the model's saturation adjustment, which governs cloud initiation and dissipation. This saturation adjustment was based on earlier cloud-scale modeling work. The model was used to simulate the Valentine's Day icing storm of 12–14 February 1990. Model results were compared to observations obtained during WISP-90. The model was able to simulate the position, timing, and peak cloud water concentration of an orographically forced supercooled liquid water cloud in good agreement with that observed by a research aircraft. The model also simulated the observed precipitation pattern well. Other features observed during this WISP-90 case such as the well-defined shallow pool of cold air and a Denver Cyclone were also reproduced in the model simulation. These features suggested that the model faithfully reproduced the overall dry dynamics of this case, thus providing the proper forcing for the moist physics parameterization.

The Valentine's Day case described in this study was a good example of how orographic forcing supported the production of SLW. However, as this simulation has indicated, other mechanisms (e.g., frontal overrunning) could be important in SLW production. More specifically, slantwise ascent might be one process that

led to the formation of SLW at higher levels in the troposphere (i.e., around 500–600 mb) in both the simulation and in the corresponding satellite imagery.

These encouraging results suggest that regional deterministic forecasting of aircraft icing is likely to be a reachable goal. However, there are several important obstacles to confront before these models become operational reality. First, the version of the microphysics parameterization used here does not permit any interaction between frozen and liquid hydrometeors (e.g., riming), which, in certain cases, can be important in the depletion of SLW. This is a serious limitation, and work continues in the pursuit of *efficient* algorithms that incorporate these processes into the mesoscale model's microphysics parameterization. Also, the partitioning into ice or liquid of newly formed cloud according to a linear function of temperature should probably undergo further examination. There might be better-suited functions to treat this process and the best function might vary from case to case (just as a particular value of  $T_{00}$  can be best for a specific case). Finally, further tests on additional cases are required before this parameterization can be considered a candidate for operational implementation.

*Acknowledgments.* We wish to thank Ms. Celia Chen (of NCAR/RAP) and Mr. James Fluke (NOAA/FSL) for gladly providing some of the essential WISP-90 data used in this study. NCAR is sponsored by the National Science Foundation. We also thank Messrs. Donald Chisholm and Mort Glass of Phillips Laboratory for useful comments and background materials, and Mr. Jeff Cutler for his capable assistance with the figures. This work was supported by the Air Force Office of Scientific Research under Projects 2310G7 and 2310CP.

## REFERENCES

- Air Weather Service, 1980: Forecaster's guide on aircraft icing. AWS/TR-80/001. [NTIS AD-A085 490/1/HDM.]
- Anthes, R. A., 1977: A cumulus parameterization scheme utilizing a one-dimensional cloud model. *Mon. Wea. Rev.*, **107**, 270–286.
- , 1983: Regional models of the atmosphere in middle latitudes. *Mon. Wea. Rev.*, **111**, 1306–1335.
- , and T. T. Warner, 1978: Development of hydrodynamic models suitable for air pollution and other mesometeorological studies. *Mon. Wea. Rev.*, **106**, 1045–1078.
- Benjamin, S. G., and N. L. Seaman, 1985: A simple scheme for objective analysis in curved flow. *Mon. Wea. Rev.*, **113**, 1184–1198.
- Davies, H. C., and R. E. Turner, 1977: Updating prediction models by dynamical relaxation: An examination of the technique. *Quart. J. Roy. Meteor. Soc.*, **103**, 225–245.
- Emanuel, K. A., 1983: On assessing local conditional symmetric instability from atmospheric soundings. *Mon. Wea. Rev.*, **111**, 2016–2033.
- , 1988: Observational evidence of slantwise convective adjustment. *Mon. Wea. Rev.*, **116**, 1805–1816.
- Errico, R. M., and G. T. Bates, 1988: Implicit normal-mode initialization of the PSU/NCAR mesoscale model. NCAR Tech. Note, NCAR/TN-312+1A. [NTIS PB88-236021/HDM.]

- Fritsch, J. M., and C. F. Chappell, 1980: Numerical prediction of convectively driven mesoscale pressure systems. Part I: Convective parameterization. *J. Atmos. Sci.*, **37**, 1722-1733.
- Hsie, E.-Y., and R. A. Anthes, 1984: Simulations of frontogenesis in a moist atmosphere using alternative parameterizations of condensation and precipitation. *J. Atmos. Sci.*, **41**, 2701-2716.
- , —, and D. Keyser, 1984: Numerical simulation of frontogenesis in a moist atmosphere. *J. Atmos. Sci.*, **41**, 2581-2594.
- Kuo, H.-L., 1974: Further studies of the parameterization of the influence of cumulus convection on large-scale flow. *J. Atmos. Sci.*, **31**, 1232-1240.
- Kuo, Y.-H., and S. Low-Nam, 1990: Prediction of nine explosive cyclones over the western Atlantic Ocean with a regional model. *Mon. Wea. Rev.*, **118**, 3-25.
- Lin, Y.-L., R. D. Farley, and H. D. Orville, 1983: Bulk parameterization of the snow field in a cloud model. *J. Appl. Meteor.*, **22**, 1065-1092.
- Lord, S. J., H. E. Willoughby, and J. M. Piotrowicz, 1984: Role of a parameterized ice-phase microphysics in an axisymmetric, nonhydrostatic tropical cyclone model. *J. Atmos. Sci.*, **41**, 2836-2845.
- Pleim, J. E., J. S. Chang, and K. Zhang, 1991: Nested grid mesoscale atmospheric chemistry models. *J. Geophys. Res.*, **96**, 3065-3084.
- Rasmussen, R. M., M. Murakami, G. Stossmeister, and B. C. Bernstein, 1991: Supercooled liquid water in Colorado Front Range winter storms: Case study of the 1990 Valentine's Day storm. Preprints, *Fourth Int. Conf. on Aviation Systems*, Paris, Amer. Meteor. Soc., 163-166.
- , M. Politovich, J. Marwitz, W. Sand, J. McGinley, J. Smart, R. Pielke, S. Rutledge, D. Wesley, G. Stossmeister, B. Bernstein, K. Elmore, N. Powell, E. Westwater, B. Boba Stankov, and D. Burrows, 1992: Winter Icing and Storms Project (WISP). *Bull. Amer. Meteor. Soc.*, **73**, 951-974.
- Sassen, K., K. N. Liou, S. Kinne, and M. K. Griffin, 1985: Highly supercooled cirrus cloud water: Confirmation and climatic implications. *Science*, **227**, 411-413.
- , C. J. Grund, J. D. Spinhirne, M. M. Hardesty, and J. M. Alvarez, 1990: The 27-28 October 1986 FIRE IFO cirrus case study: A five lidar overview of cloud structure and evolution. *Mon. Wea. Rev.*, **118**, 2288-2311.
- Szoke, E. J., M. L. Weisman, J. M. Brown, F. Caracena, and T. W. Schlatter, 1984: A subsynoptic analysis of the Denver tornado of 3 June 1981. *Mon. Wea. Rev.*, **112**, 790-808.
- Tao, W.-K., J. Simpson, and M. McCumber, 1989: An ice-water saturation adjustment. *Mon. Wea. Rev.*, **117**, 231-235.
- Zhang, D.-L., 1989: The effect of parameterized ice microphysics on the simulation of vortex circulation with a mesoscale hydrostatic model. *Tellus*, **41A**, 132-147.
- , and R. A. Anthes, 1982: A high resolution model of the planetary boundary layer—Sensitivity tests and comparison with SESAME-79 data. *J. Appl. Meteor.*, **21**, 1594-1609.
- , H.-R. Chang, N. L. Seaman, T. T. Warner, and J. M. Fritsch, 1986: A two-way interactive nesting procedure with variable terrain resolution. *Mon. Wea. Rev.*, **114**, 1330-1339.
- , E.-Y. Hsie, and M. W. Moncrieff, 1988: A comparison of explicit and implicit predictions of convective and stratiform precipitating weather systems with a meso- $\beta$  scale numerical model. *Quart. J. Roy. Meteor. Soc.*, **114**, 31-60.

Accession For	
NTIS GRA&I	<input checked="" type="checkbox"/>
DTIC TAB	<input type="checkbox"/>
Unannounced	<input type="checkbox"/>
Justification	
By _____	
Distribution _____	
Availability Codes	
Dist	Avail and/or Special
A-1	20